ACS APPLIED NANO MATERIALS

www.acsanm.org
Article

Freestanding Porous Silicon Membranes for Sensing Enabled by Flow-Through Decoration of Gold Nanoparticles

Clémentine Gevers, Louise Lejeune, Eléonore Masarweh, Sophie Hermans, and Laurent A. Francis*

Cite This: ACS Appl. Nano Mater. 2025, 8, 21285−21293
Read Online

ABSTRACT: Tuning and optimizing the optical, physical, and chemical properties of porous silicon (PSi) by decoration with plasmonic nanoparticles (NPs) are a trending yet challenging topic. The current NPs deposition methods tend to cluster them on top of the pores instead of maximizing the plasmonic effect by homogeneous distribution inside the pores. Here, a novel flow-through strategy is introduced to homogeneously decorate PSi freestanding membranes (FSM) with a colloidal NPs suspension. FSM offers high ease of fabrication, but the main current challenges are low repeatability and difficult microfluidic integration. We used a numerical simulation to determine the main fabrication parameters, unlocking the reliable release of FSM with very large pores up to 67 nm. To enable the flow-through, the FSM was subsequently integrated into a microfluidic cell using a flexible Kapton holder. Solving these challenges allowed us to fully decorate the pores with presynthesized Au NPs and obtain a homogeneous decoration of the whole FSM thickness. As a representative application, reflective interferometric Fourier transform spectroscopy (RIFTS) measurements demonstrated enhanced sensing performance with both increased sensitivity and reduced standard deviation. These results highlight the potential of decorated FSM as versatile substrates for plasmonic, catalytic, sensing, and other nanophotonic applications.

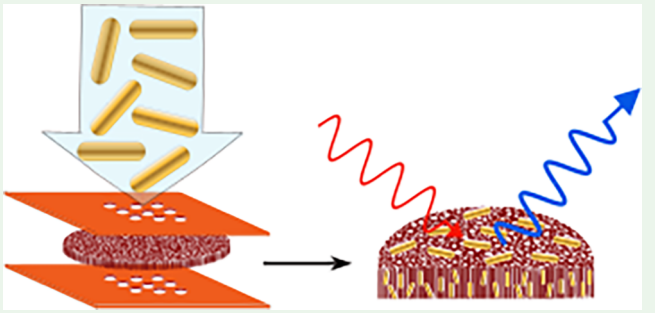

KEYWORDS: *porous silicon, freestanding membrane, plasmonic nanoparticles, pore size, flow-through, optical sensing*

1. INTRODUCTION

Since the late 1980s, porous silicon (PSi) has been of interest to the scientific community for its many optical properties.[1] But it has been given lately additional attention since its hybridization by integration with plasmonic nanoparticles (NPs) that increase its optical, physical, and chemical properties and open the door to many applications. Indeed, the chemical and physical properties[2] of NPs are not only controlled by their sizes and shape but are also dependent on their surrounding environment that dictates their plasmonic behavior. They can improve the physical properties of semiconductors and more specifically PSi.[3] The optical response of PSi can be tuned by NPs thanks to the strong localized electromagnetic fields near the surface of plasmonic NPs.[3] This behavior arises from the collective excitation of the electrons in the metal responsible for the formation of the surface plasmons. Therefore, the local resonance occurs at the interface between PSi and NPs and enhances the coupling efficiency of light because of enhanced optical scattering.[4]

This filling of PSi with plasmonic NPs is thus a hot topic and has been used recently in many promising application fields, including enhanced photovoltaics,[5] catalytic activity,[2,6,7] antireflective coatings,[4] enhanced light emission in optoelectronic devices,[8−12] antibacterial activity,[13] computerized tomography imaging,[14] surface-enhanced Raman,[15−17] or infrared absorption spectroscopy,[18−25] as well as enhanced interferometric performance in (bio)sensing applications.[26]

The decoration of the silicon pores by NPs has been demonstrated in several ways, as reviewed by Khinevich et al.[27] It is possible to synthesize the NPs in situ through the immersion deposition,[7,11,12,18,19,21,25,28] where the weak Si−H bonds are used to reduce impregnated metallic ions into metal NPs. This galvanic immersion plating method is usually chosen because of its simplicity, but NPs typically form clusters on the surface[11] with poor control over their shape. In addition, there is only minor penetration of the deposited NPs into the thickness of the pore system.[19] Some authors proposed to oxidize the PSi to enhance its hydrophilicity and thus increase the amount of NPs synthesized inside the pores.[12,14] By opposition, the pores can be decorated by depositing metallic NPs from their colloidal suspensions.[27] The main advantage of

Received: August 4, 2025
Revised: October 3, 2025
Accepted: October 6, 2025
Published: October 23, 2025

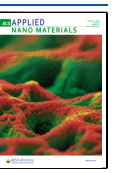

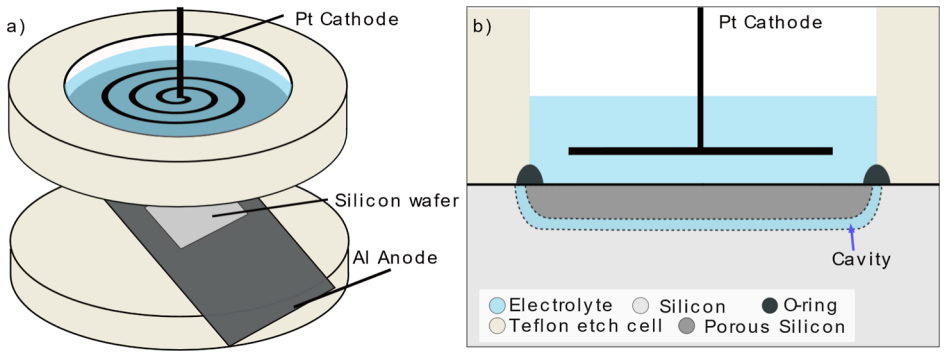

Figure 1. a) Exploded view of an electrochemical etching cell, with a Teflon etch cell, an aluminum foil as anode, a silicon wafer, and a platinum spiraled wire that is the cathode; (b) cross section of the etch cell after the formation of the cavity.

Table 1. Comparison of FSM from the Literature Based on Pore Size

mean pore size top	electropolishing current	etch time	decoration	ref
3−8 nm	13−27 mA/cm^2	1.5 s		Chen[33]
10 nm				Terheiden[53]
10 nm	250 mA/cm^2			Solanki[32]
6−17 nm	220 mA/cm^2			Jubgang[54]
20 nm	50 mA/cm^2	30 s		Liu[55]
20 nm	4 mA/cm^2	95 s	immersion plating	Novara[38,39]
20−30 nm	600 mA	few seconds		De La Luz-Merino[56]
2−30 nm	450 mA	60 s		Velleman[57]
30 nm	45 mA/cm^2	15 s		Martin-Sanchez[40]
35 nm	800 mA/cm^2	0.1 s		Corsi[42]
30−40 nm	22 mA/cm^2	180 s	colloidal NPs	Jin[13]
20−60 nm	76 mA/cm^2	6 s	immersion plating	Bu[18]
40 nm	200 mA/cm^2	pulse		Cencha[58]
40−80 nm	high	pulse		Pei[59]
52 nm	170 mA/cm^2	60 s	immersion plating	Vendamani[21]
67 nm	**800 mA/cm^2**	**3 s**	**colloidal NPs**	**this work**
0.5−2 μm	2−15 mA/cm^2	10 min/step		Thakur[35]

this method compared to all other in situ techniques is that the size and shape of the NPs can be well controlled by prior wet synthesis targeted for the desired applications. Noncovalent chemistry can be used to reach electrostatic interactions, as exemplified by the layer-by-layer technique proposed by Mariani et al.[26] for the nanoassembling of gold NPs (Au NPs) onto silicon dioxide. Another method is the silanization[15] of the PSi with aminopropyltriethoxysilane as a linker for Au NPs. However, most of the decorated PSi substrates are prepared via drop-casting[3,5,9,29] of the nanoparticle suspension, which typically results in the formation of a metallic crust on the surface. This crust can result in clogging of the pores rather than filling them because of the hydrophobic character of PSi.[3] The deposition is typically inhomogeneous and exhibits a coffee-ring pattern, which is influenced by the porosity and oxidation state of the PSi.[3]

The common problem with most of these methods is that the NPs are mainly on top of the PSi and not trapped inside the pores, while a higher plasmon effect has been shown when Au NPs are uniformly distributed in the pores.[12,15] The mobility being higher outside the pores, NPs deposited on the outer surface also tend to form clusters that cannot be controlled. This is why we propose here an innovative solution enabling the flow of Au NPs through PSi membranes to decorate the totality of the thickness of the PSi layers. To do so, we propose to use freestanding membranes (FSM) because of their quick and simple fabrication method compared to traditional membranes, which combine wet, dry, and electrochemical etching for the critical step of release.[1] FSM prepared by electrochemical etching involves a two-step process. First, a layer with the desired porosity for the final membrane is created. Then, a high porosity layer is produced, which is brittle and coalesces into a cavity under the first layer to facilitate the membrane's mechanical detachment in a step named lift-off. This is represented in Figure 1, where Figure 1a shows the etch cell and Figure 1b locates the cavity. After this phase, the freestanding layer can be transferred onto another substrate, such as a tape or polymer slab, for implementation in different applications. The remaining bulk silicon substrate can be reused afterward.[30]

Since the early 2000s, multiple methods to fabricate FSM by electrochemical etching have been explored. The electrochemical etch involves wet etching of monocrystalline silicon by applying an electric current at the electrodes in the presence of an HF-containing electrolyte,[31] this setup is shown in Figure 1a. Solanki et al.[32] proposed a two-step procedure, where the current applied is increased after the first anisotropic layer is etched. This allows one to rapidly increase the pore size and thus generates the cavity, causing lift off,[33] as this isotropic etch interconnects the pores that finally merge into a single void.[32] These pores will eventually overlap together and fracture from the bulk.[34,35]

The key is to apply a sufficiently high current such that the mass transfer rate of the fluoride ion is lower than the delivery

https://doi.org/10.1021/acsanm.5c03632
ACS Appl. Nano Mater. 2025, 8, 21285−21293

rate of valence band holes at the Si/PSi interface. The shortage of fluoride ions leads to the formation of SiO_2 instead of the soluble SiF_4 and the reaction stoichiometry transitions from 2 electrons (eq 1) to 4 electrons (eq 2)[31]

$$Si + 6HF + 2h^+ \rightarrow SiF_6^{2-} + 4H^+ + H_2 \quad (1)$$

$$Si + 6HF + 4h^+ \rightarrow SiF_6^{2-} + 6H^+ \quad (2)$$

This oxide layer grows further at the interface and blocks the electrochemical current; this results in the thinning of the pore walls. Eventually, the oxide layer is dissolved by HF, leading to the detachment of the porous layer.[31] This mechanism is called electropolishing.

In the case of incomplete lift-off, the membrane can still be detached subsequently mechanically either on a tape, as reported by Bardet et al.,[30] or on polydimethylsiloxane[36−41] (PDMS). Some mechanical force can also be applied, such as a water jet, ultrasonic vibration, or mechanical tensile force.[32] Another way to induce the detachment is to score and release the edges of the patterned film before the second anodization using a stainless-steel syringe.[36,41,42]

The main disadvantage of PSi FSM is the low repeatability of the procedure and the fragility of the resulting membrane that limits the integration in a microfluidic setup, as mentioned by Zhao et al.[43] The control of large pore size is another challenge,[31] notably with p-type Si substrates, which are preferred for their compatibility with electronics applications. To the best of our knowledge, FSMs have reached average pore sizes of 50 nm at the maximum, as shown in Table 1, which compares the mean pore size of FSM in the literature but not the thickness, as it is a less critical parameter because it mainly depends on the etch time. This limitation in pore size hinders the flow of liquids or NP suspensions through the membrane. A final problem of current PSi FSM fabrication methods is related to near-edge porosity that poses specific problems as it varies due to restricted electrolyte diffusion and nonuniform current density under the O-ring seal during the electrochemical etch.[44] This leads to difficulty in reproducing the shape of the FSM and problems of integration in a microfluidic setup.[43]

Building on the identified limitations of the existing state of the art, this work aims to develop an Au NP-decorated PSi FSM, either in a single- or even double layer setup to measure the enhanced optical sensitivity of the FSM. To achieve this, we analyze the critical fabrication steps required to produce PSi FSM with large pores, aiming for both reproducibility and microfluidic compatibility. This methodology facilitates the design of a system that enables efficient fluid transport, thereby optimizing decoration of the full thickness of the porous layer with a colloidal Au NPs suspension.

2. MATERIALS AND METHODS

2.1. Materials and Chemicals. Single-side polished, boron-doped (p-type) silicon wafers (<2 mΩ cm, 381 ± 20 μm, <100> ± 1° orientation, 76.2 ± 0.3 mm diameter) (SIEGERT WAFER GmbH), absolute ethanol (EtOH, AnalR NORMAPUR Reag. Ph. Eur., VWR Chemicals), aqueous hydrofluoric acid (HF, 49%, Chem-Lab NV), hexadecyltrimethylammonium bromide (CTAB, ≥98%, Sigma-Aldrich), hydrochloric acid (HCl, VWR Chemicals), hydrogen tetrachloroaurate hydrate ($HAuCl_4$, 99.999%, trace metal basis, Thermo Scientific Chemicals), hydroquinone (99%, Sigma-Aldrich), nitric acid (HNO_3, 65%, analytical reagent grade, Fisher Chemical), potassium hydroxide (KOH, >85% for laboratory use, Ph. Eur., Chem-Lab NV), silver nitrate ($AgNO_3$, ≥99%, ASC reagent, Sigma-Aldrich), and sodium borohydride ($NaBH_4$, ≥98%, Sigma-Aldrich) were used as received.

2.2. Preparation of PSi Membranes:Single and Double Layers. In this study, a p-type Si substrate of 1 mΩ·cm (resistivity measured using a 4-point probe) is etched, with an electrolyte solution used for each etching step being a solution of HF (49% aqueous): ethanol (3:1 v/v). The sacrificial step consists of etching a sacrificial porous layer at 300 mA/cm^2 for 60 s and removing it with a 2 M solution of KOH for 5 min. Since porous silicon dissolves in strongly basic media, this step provides a rapid and effective cleaning of the surface. By eliminating the initial irregularities, the subsequent porosification proceeds more uniformly, leading to improved reproducibility and a narrower pore size distribution.[31] Then, for the single-layer FSM, an etching step is carried out at a constant current density of 300 mA/cm^2 for 360 s. After an etch stop of 3 s, a current density of 800 mA/cm^2 is applied for 3 s. The FSM is then rinsed three times with isopropanol before being glided onto the Kapton holder. This entire process is completed under 25 min and gives a porosity of around 70% (measured by the spectroscopic liquid infiltration method, SLIM, as described in Supporting Information 1.2) and an estimated membrane thickness of 57 μm (more details in Supporting Information 1.1). The membrane is then oxidized at 200 °C for 1 h under an ambient atmosphere to stabilize the oxidation of the FSM. The double-layer FSM structures are fabricated following the same protocol as the single-layer samples, with the exception of the anodization sequence following the sacrificial etch step: a current density of 300 mA/cm^2 is applied for 19 s, followed by an etch stop of 3 s. A second anodization is then performed at 100 mA/cm^2 for 783 s. Upon release, the resulting FSM comprises a first porous layer with approximately 70% porosity and a thickness of 3 μm, followed by a second layer with 55% porosity and a thickness of 54 μm. 50 single-layer FSMs and 25 double-layer FSMs were prepared, which demonstrates the repeatability of the process.

2.3. COMSOL Simulation. A finite element simulation (FEM) on COMSOL Multiphysics software version 6.1, in the electrodeposition physics based on Ivanov's methodology,[45,46] analyses the behavior beneath the O-ring. For the input parameters of the model, the stoichiometry of eq 2 was set to obtain the etch rate. A high current density of 800 mA/cm^2 was applied to simulate the electropolishing step. In order to find a solution, a time step of 10 μs was applied (more details in Supporting Information 2).

2.4. Sample Characterization. The morphology of the PSi was analyzed using a Scanning Electron Microscope, Zeiss Auriga FIB-SEM, at an acceleration voltage of 3 kV. The count of the NPs was done with a homemade Python code that uses adaptive thresholding to detect the white spherical NPs based on contour detection. An interactive feature was added to the code to allow the user to remove some miscounted NPs and to add the ones that were not detected. The full code, together with usage instructions, is available in a public repository (https://github.com/clementinegevers/Count-NPs-in-PSi). For further analyses of nanoparticle morphology, such as shape and size distributions, ImageJ remains a well-established and reliable alternative. Optical characterization of the PSi double layer was done through fast Fourier transform reflectance spectroscopy, where PSi layers were optically characterized in air (450−850 nm) by using a fiber-optic Ocean Optics JAZ spectrometer and a 10 mW halogen light source. Acquisition parameters of reflection spectra were as follows: integration time of 1.5 ms, average scan number 3. The measured spectra were normalized with respect to a reference mirror (broadband mirror, Thorlabs, USA).

2.5. Nanoparticles Synthesis Protocol and Characterizations. Gold nanorod suspension used in the microfluidic experiment was prepared by a seed-mediated protocol, where silver nitrate is included to direct anisotropic growth by selectively adsorbing on specific crystal facets, promoting the elongation of the gold nanorods,[47−49] explained in more detail in Supporting Information 3. The characterizations were done through UV−vis spectroscopy and Transmission Electron Microscopy; these measurements are shown in Supporting Information 4.

https://doi.org/10.1021/acsanm.5c03632
ACS Appl. Nano Mater. 2025, 8, 21285−21293

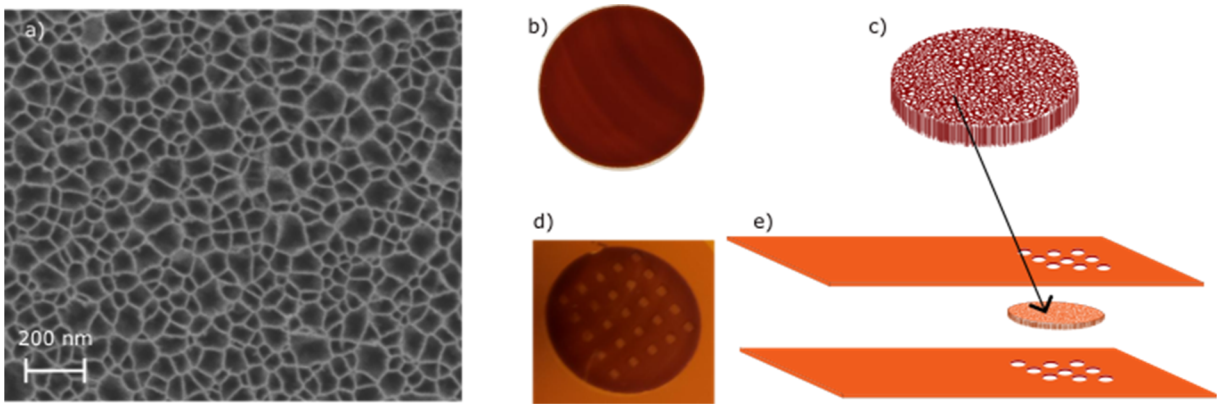

Figure 2. (a) SEM image of the top of the FSM prepared at a current density of 300 mA/cm^2, with a magnification of 37.23k×, the pores have an average size of 67 nm; (b) top-view photography of the top of an FSM of 1.2 cm^2; (c) schematic image of an FSM extruded from Figure 2a; (d) FSM sandwiched inside the Kapton holder; and (e) exploded schematic view of the FSM in the Kapton holder.

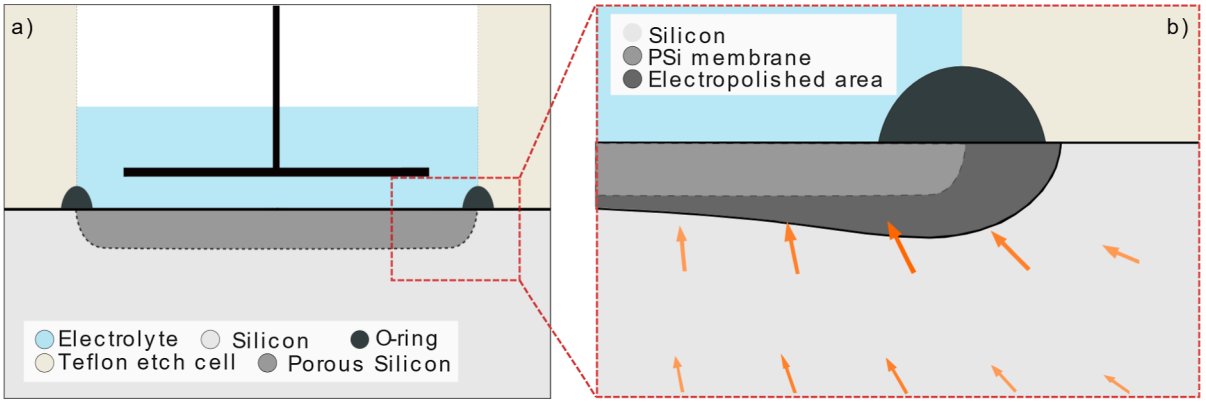

Figure 3. Cross-section views of a simulated electrochemical etch: (a) after the first anodization step; (b) zoom of the simulated etch front of the electropolished underetch below the O-ring during the second anodization step. Orange arrows represent the electrode current density from the aluminum electrode, and the gradient of the arrows shows the intensity of the current density.

3. RESULTS AND DISCUSSION

3.1. Anodization of Large Pore Size and Controlled Release of the FSM. The choice of working with highly doped p-type silicon is justified by the possibility of reaching large pores.[31] This enables us to synthesize bigger Au NP sizes that can still flow through it. After characterizing the substrate at different current densities and by measuring the porosity and pore size (see Supporting Information 1.2), it was found that at a current density of 300 mA/cm^2, the pores have a mean size of 67 ± 38 nm, as shown in Figure 2a and detailed in Supporting Information 1.2. This average size of 67 nm is large for FSMs compared to the state of the art, as shown in Table 1.

To increase the reproducibility of the FSM preparation, we needed to better understand and improve the release process from the substrate. To do so, an FEM on COMSOL Multiphysics software is used to analyze the electropolishing step after the anisotropic etch (see Supporting Information 2). This simulation, based on Ivanov's methodology,[45] analyzes the behavior beneath the O-ring as the porosity varies at the edges. Figure 3a illustrates the porosification after the initial step, while Figure 3b depicts the electropolished region beneath the O-ring after 3 s of etching. The arrows indicate the direction of the electrode current density, and the gradient represents its intensity, demonstrating that the area beneath the O-ring is etched more rapidly than the surrounding regions due to current crowding.[45]

This observation aligns well with the experimental results. By varying the electropolishing duration, we noted that an insufficient electropolishing time prevents membrane detachment, whereas excessive electropolishing induces membrane breakage at the border near the O-ring. Therefore, an optimal electropolishing time must be determined to ensure complete lift-off of the membrane without compromising its structural integrity at the edges. This is shown in Supporting Information 1.4.

Knowing this, our PSi FSM fabrication process follows the simple approach outlined in Corsi's work,[42] except omitting the mechanical step of scratching the edge of the FSM to separate it from bulk silicon. We use a controlled electropolishing time of 3 s instead, ensuring a clear and reproducible release of the FSM at the surface of the electrolyte solution. A top view of the so-obtained FSM is shown in Figure 2b.

After a few seconds of electropolishing, the lift-off detachment of the porous membrane can be observed as a sudden voltage drop measured with a Keithley 2450 source measure unit. This phenomenon corresponds to the rupture of the silicon substrate and the FSM.[34] Immediately after, the voltage rises again, indicating the formation of a new PSi layer on the substrate (Supporting Information Figure S5). Similar observations have also been reported in the literature.[33,34,50]

The choice of a 3 s electropolishing step has been found as the optimized trade-off, ensuring both systematic release and

https://doi.org/10.1021/acsanm.5c03632
ACS Appl. Nano Mater. 2025, 8, 21285−21293

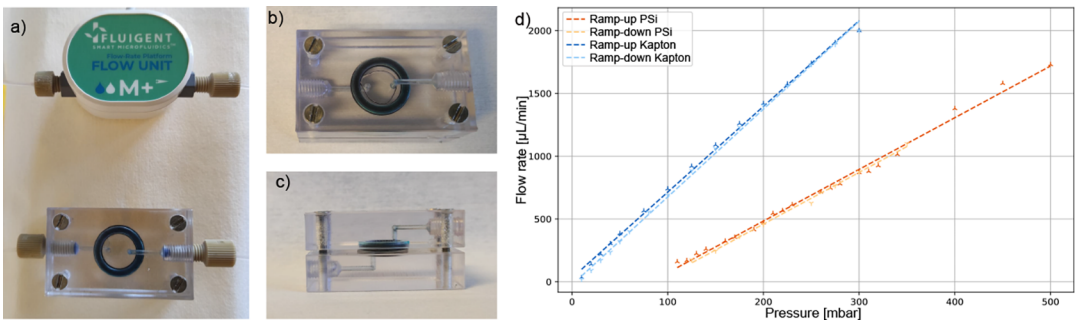

Figure 4. (a) Picture of the microfluidic setup, showing the Fluigent flow unit that measures the flow rate upstream of the cell; Microfluidic cell: (b) top view, (c) side view, and (d) plot of the pressure versus the flow rate for the rise (dark markers) and drop (light markers) of the pressure with their respective linear regression (dashed curves), for the Kapton holder alone (blue) and single-layer FSM (red), with a respective slope of 6.9 μL/min/mbar and 4.1 μL/min/mbar.

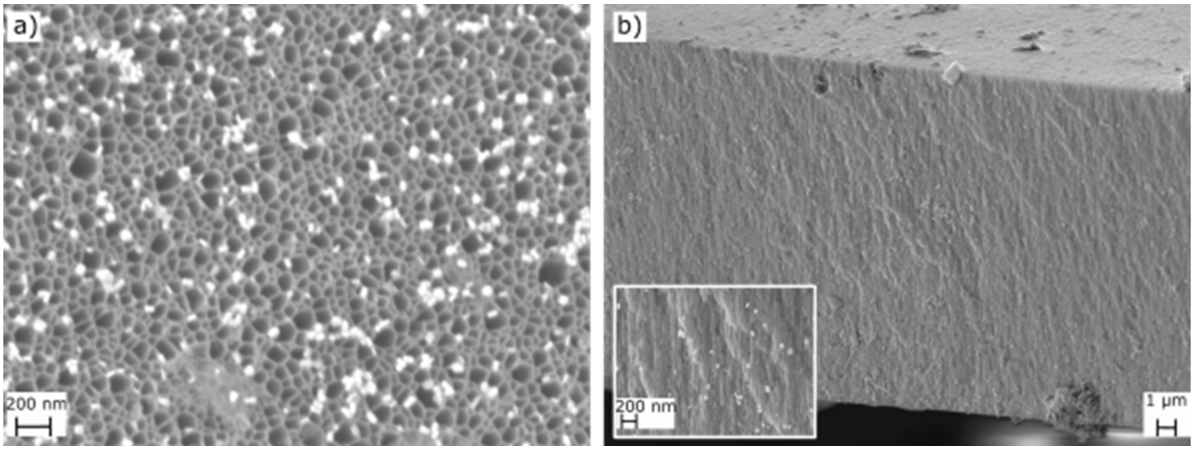

Figure 5. SEM images of decorated FSM with Au NPs; (a) top view of the FSM with a magnification of 26.33k×; (b) cross-section view of the whole thickness of the FSM with a magnification of 3.27k×; the inset is a zoom of the center of it with a magnification of 41.27k×. The Au NPs are clearly observable in white.

reproducible shape defined by the O-ring, giving in our case a disk of 6.2 mm in diameter (more details in Supporting Information 1.4).

The FSM was subsequently integrated into a homemade Kapton holder (DuPont de Nemours inc., see Supporting Information 1.3) that was perforated by CNC cutting. Kapton is a polyimide sheet with heat resistance up to 400 °C, making it a suitable material for the thermal processes involved during the whole fabrication. This holder eases the manipulation of the FSM. It also increases the process compatibility, the flexibility, and the mechanical strength of FSM. The integration of the FSM within the holder is shown in Figure 2c–e.

3.2. Microfluidic Integration. The microfluidic setup wherein the Kapton holder can be placed is shown in Figure 4a–c. The Kapton holder shape helps to limit the stress that is applied to the FSM when fastening the screws of the microfluidic cell.

The flow rates of DI water in the empty Kapton holder and for the Kapton holder with the single-layer FSM have been measured at different pressure values with a Fluigent LINEUP fluidic setup (see Figure 4a). The linear relation of 6.9 and 4.1 μL/min/mbar was obtained for the empty holder and with the FSM, respectively, as shown in Figure 4d, where the same relation can be seen at the increase and decrease of the pressure. This is in accordance with Darcy's law.[51]

To reach a flow of 20 μL/min, a pressure of 40 mbar is needed, as shown in Supporting Information 5. This is a lower pressure than typical pressure applied on PSi membranes so far; for instance, for a flow of 15–20 μL/min, Vercauteren et al.[1] reported that a pressure of 2 bar needs to be applied due to the smaller PSi pore size of 12–20 nm. To compare the impact of the pore size, the flow through the double layer has also been measured. The linear relation is then 0.01 μL/min/mbar for the double layer (see Supporting Information 5). The observed flow through the membrane with 20 nm pores is approximately 400 times lower than that of the membrane with 67 nm pores. This strong dependence is well described by the Hagen–Poiseuille equation, which predicts that the volumetric flow rate Q through a cylindrical pore scales as $Q \propto 1/r^4$, where r is the pore radius. Given this fourth-power relationship, even modest increases in the pore size lead to substantial increases in flow. The ratio of 67 nm over 20 nm to the fourth power corresponds to 126, which is on the same order of magnitude as the measured slope ratio between the two. Consequently, working with larger pores is advantageous as a lower pressure is required to achieve a given flow rate.

3.3. Benchmarking of the Decoration. Thanks to our designed Kapton holder, PSi FSM are easily inserted into the microfluidic cell, allowing a controlled flow of presynthesized Au nanorods suspension (cf. Supporting Information 3–4) through the pores, leading to their deposition within the whole porosity. We chose nanorods, as they allow increased

https://doi.org/10.1021/acsanm.5c03632
ACS Appl. Nano Mater. 2025, 8, 21285–21293

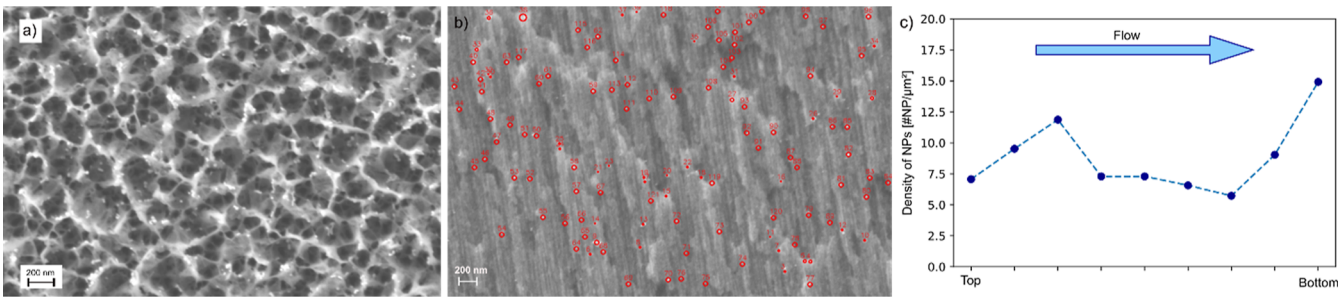

Figure 6. (a) Back view of the FSM with a magnification of 31.95k×; (b) cross-section view of the FSM with a magnification of 22.67k×, where the red dots show the automatic detection by the Python code and count the amount of detected Au NPs; and (c) evolution of the density of the NPs through the whole thickness of the membrane, showing the direction of the flow of Au NPs, it can be concluded that the totality of the membrane is decorated.

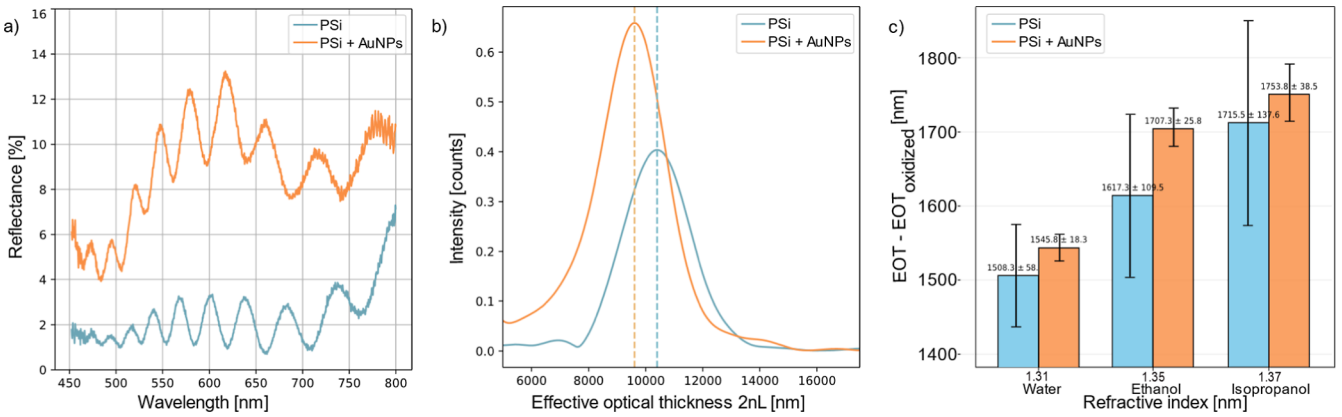

Figure 7. (a) Reflectance spectra of an oxidized FSM double layer, before (blue) and after (orange) decoration with Au NPs; (b) corresponding Fourier transform spectra; the values of the effective optical thickness of the FFT peak for each spectrum are 10403 (PSi) nm and 9607 nm (PSi + Au NPs), showing the blueshift; (c) histogram showing the effective optical thickness (EOT) shift of oxidized porous silicon (PSi) membranes with (orange) and without (blue) gold NPs as a function of the refractive index of the infiltrated liquid (water, ethanol, and isopropanol). The vertical bars show the standard deviation of each measure.

plasmonic effect compared to spherical particles and require prior synthesis, as anisotropic nanoparticle shapes cannot be obtained by any in situ reduction/deposition techniques; moreover, gold offers high chemical stability, although other plasmonic materials such as silver or copper could also be employed.

To the best of our knowledge, no porosified Si membrane has previously been decorated in this way with presynthesized Au NPs inside the pores, even spherical ones.

These Au NPs were injected at a pressure of 40 mbar. Figure 5a shows the top view of the decorated membrane, and Figure 5b demonstrates that the flow of Au NPs went through the membrane, as we imaged a cross-section of the decorated FSM where nanorods are visible all along the thickness of the membrane with a homogeneous distribution. The bright white spots observed in Figure 5 correspond to Au nanoparticles and not residuals, as confirmed by XPS analysis (Supporting Information 6.3).

When looking at the back of the FSM, we can also see NPs, showing that the NPs fully decorate the totality of the membrane. This is shown in Figure 6a. To validate this, the amount of NPs in the FSM was counted with a homemade Python code that uses adaptive thresholding to detect the white spherical NPs based on contour detection. An example is shown in Figure 6b, and more is shown in Supporting Information 6. The evolution of the density of particles through the whole FSM is shown in Figure 6c, which allowed us to calculate a mean density of 8.47 #NP/μm^2.

By working with this microfluidic setup instead of a drop-casting method, we can show that the synthesized NPs are homogeneously dispersed inside the pores as it follows the flow through the pores and no coffee ring effect is present; this has been validated by XPS measurement (cf. Supporting Information 6.3). We also prepared a decorated FSM with the drop-casting method for comparison purposes (cf. Supporting Information 6.2). In this case, no NPs were counted inside the FSM, showing the utility of the flow-through technique to decorate the membrane.

A final reflectance measurement was performed on the decorated double-layer membrane to evaluate the optical impact of Au NPs on the interference fringes and better understand the penetration of the NPs. As shown in Figure 7a, the intensity of the reflected signal increases after decoration. This enhancement can be attributed to the mirror-like effect[26] of the Au NPs deposited on top of the FSM; these NPs are shown in Figure 5a. In addition, a notable blue-shift in the Fast Fourier Transform (FFT) of the reflectance is observed, as shown in Figure 7b. The measured shift of 796 nm indicates that Au NPs infiltrated the porous matrix, since the refractive index of gold is lower than air in the visible range and induces a reduction of the effective refractive index of the porous matrix. Interestingly, the magnitude of the measured blueshift is substantially larger than what has been reported before; for

https://doi.org/10.1021/acsanm.5c03632
ACS Appl. Nano Mater. 2025, 8, 21285−21293

instance, Jiao et al.[15] documented a blueshift of only 85 nm. The greater shift measured in this work likely results from the complete and uniform integration of Au NPs throughout the FSM. To further support this interpretation, we performed optical simulations using the transfer matrix method[15,26] with the Bruggeman effective medium approximation[52] for oxidized porous silicon. The calculations reproduced a blue shift when Au nanoparticles were placed inside the pores, in agreement with our measurements, whereas modeling a continuous gold layer deposited only on the surface of the membrane resulted instead in a ∼200 nm redshift. This clear difference validates that the inner pores were decorated with gold nanorods.

Reflective interferometric Fourier transform spectroscopy (RIFTS) measurements were performed to evaluate the sensing performance of double-layer FSMs with and without Au nanorod decoration. The effective optical thickness (EOT) was measured upon infiltration with liquids with different refractive indices. The results are shown in Figure 7c and demonstrate that the EOT shift is more pronounced for decorated membranes compared to undecorated ones, indicating an increased sensitivity of the sensor after nanoparticle infiltration. In addition, the standard deviation of the measurements is consistently reduced in the decorated samples, demonstrating improved reproducibility. This simultaneous enhancement in sensitivity and reduction in variability highlights the potential of decorated FSMs as promising platforms for plasmonic sensing applications.

Table 1 summarizes different p-type FSMs based on the size of the pores. These range from a few nanometers to micrometers. With our methodology, the mean pore size is in the upper range. As can be seen with the different electropolishing currents and etch times, the methodology for the release of the FSM is specific to each work.

As listed in Table 1, most of the FSM decoration is done through the immersion plating method.[18,21,38,39] In contrast, Jin et al.[13] achieve pore infiltration using a colloidal suspension. In their approach, the FSM is fragmented into flakes via ultrasonication before being mixed with the NPs suspension, effectively enabling full penetration. The method presented in this work offers a novel alternative, enabling the integration of presynthesized colloidal nanoparticles with controlled size and shape directly into intact freestanding membranes. This opens the door to applications where the FSM needs to be integrated into a flow-through system too.

4. CONCLUSION

In conclusion, a fast and straightforward fabrication method has been developed to prepare a PSi FSM with large pores of about 67 nm that is encapsulated in a Kapton holder that brings mechanical strength and allows integration inside a microfluidic setup. The FEM simulation helped to understand the current crowding under the O-ring and fixed the electropolishing time to 3 s, allowing us to obtain a repeatable FSM shape. Thanks to the relatively large pore size, the pressure required for the Au NPs suspension to flow through the membrane is only 40 mbar, and it was shown that the Au NPs were not clogging the pores but decorated the whole surface inside the pores, with a mean density of 8.47 #NP/μm^2 through the whole thickness. The pore size of the FSM can be adapted during the anisotropic etch. To demonstrate application potential, RIFTS measurements were performed. These revealed that the EOT shift was more pronounced for decorated membranes compared to undecorated ones, confirming an increase in sensitivity, while the standard deviation of the measurements was simultaneously reduced, indicating improved reproducibility. This dual improvement highlights the promise of decorated FSMs for plasmonic sensing. Altogether, the versatility of this device would ease the functionalization of the membrane with diverse nanoparticles or chemical reactants, paving the way for its use as a substrate in catalytic, plasmonic, or multifunctional nanodevices in flow-through mode if necessary.

■ ASSOCIATED CONTENT

Supporting Information

The Supporting Information is available free of charge at https://pubs.acs.org/doi/10.1021/acsanm.5c03632.

Additional information about the list of chemicals that were used for the fabrication of the FSM and Au NPs, preparation of PSi FSM and more precisely its fabrication protocol, COMSOL simulation model, characterization of PSi, fabrication of the Kapton holder, impact of the time of the electropolishing step, protocol of the Au NPs synthesis, characterization of these Au NPs, microfluidic measurements, and characterization of the decoration method (PDF)

■ AUTHOR INFORMATION

Corresponding Author

Laurent A. Francis − *Institute for Information and Communication Technologies, Electronics and Applied Mathematics (ICTEAM), UCLouvain, Louvain-la-Neuve 1348, Belgium;* orcid.org/0000-0003-4683-3916; Email: laurent.francis@uclouvain.be

Authors

Clémentine Gevers − *Institute for Information and Communication Technologies, Electronics and Applied Mathematics (ICTEAM), UCLouvain, Louvain-la-Neuve 1348, Belgium;* orcid.org/0000-0002-2722-7438

Louise Lejeune − *Institute of Condensed Matter and Nanosciences (IMCN), UCLouvain, Louvain-la-Neuve 1348, Belgium*

Eléonore Masarweh − *Institute for Information and Communication Technologies, Electronics and Applied Mathematics (ICTEAM), UCLouvain, Louvain-la-Neuve 1348, Belgium*

Sophie Hermans − *Institute of Condensed Matter and Nanosciences (IMCN), UCLouvain, Louvain-la-Neuve 1348, Belgium;* orcid.org/0000-0003-4715-7964

Complete contact information is available at: https://pubs.acs.org/10.1021/acsanm.5c03632

Author Contributions

The manuscript was written through the contributions of all authors. All authors have given approval to the final version of the manuscript.

Funding

This research was funded by the Belgian National Fund for Scientific Research (FRIA PhD grant to C.G. n°5107123F).

Notes

The authors declare no competing financial interest.

■ ACKNOWLEDGMENTS

The authors thank the staff of the Winfab cleanroom and Welcome characterization technological platforms at UCLouvain for their technical support. They also thank Elia Colomer Clavel for her work on the characterization of the porous silicon and Lauraleen Barremaecker for XPS measurements and data analysis.

■ REFERENCES

(1) Vercauteren, R. *Porous Silicon FLow-through Membrane: Application to the Optical Detection of Bacteria from their Lysate*; UCLouvain, 2022.
(2) Liang, L.-Y.; Kung, Y.-H.; Hsiao, V. K. S.; Chu, C.-C. Reduction of Nitroaromatics by Gold Nanoparticles on Porous Silicon Fabricated Using Metal-Assisted Chemical Etching. *Nanomaterials* **2023**, *13* (11), 1805.
(3) De La Mora, M. B.; Bornacelli, J.; Nava, R.; Zanella, R.; Reyes-Esqueda, J. A. Porous Silicon Photoluminescence Modification by Colloidal Gold Nanoparticles: Plasmonic, Surface and Porosity Roles. *J. Lumin.* **2014**, *146*, 247−255.
(4) Ge, D.; Fang, Z.; Zhao, C.; Shi, J.; Zhang, L. Preparation and Anti-Reflection Performance of Porous Silicon/Gold Nanocomposite Structures. *Eur. Phys. J. D* **2023**, *77* (6), 108.
(5) Khalifa, M.; Jaduaa, M.; Abd, A. Quantum Dots Gold Nanoparticle/Porous Silicon/Silicon for Solar Cell Applications. *J. Nanostruct.* **2020**, *10* (4), 863.
(6) Ciemięga, A.; Maresz, K.; Romaszewski, M.; Głomb, P.; Krupska-Wolas, P.; Prusik, K. Hyperspectral Imaging as a Facile and Non-Destructive Method for Size Analysis of Gold Nanoparticles Deposited on Porous Materials. *Part. & Part. Syst. Charact.* **2024**, *41* (2), 2200204.
(7) Dheyab, A. B.; Alwan, A. M.; Zayer, M. Q. Optimizing of Gold Nanoparticles on Porous Silicon Morphologies for a Sensitive Carbon Monoxide Gas Sensor Device. *Plasmonics* **2019**, *14* (2), 501−509.
(8) Ramadan, R.; Martín-Palma, R. J. The Infiltration of Silver Nanoparticles into Porous Silicon for Improving the Performance of Photonic Devices. *Nanomaterials* **2022**, *12* (2), 271.
(9) Hmmoodi, A. M.; Nayef, U. M.; Rasheed, M. Nano-Gold via Laser Ablation in Liquid at Different Laser Energies on Porous Silicon for Photodetector Application. *J. Opt* **2024**, 1−8.
(10) Severiano, F.; Gayou, V. L.; García, G.; Luna-López, J. A.; Gutiérrez, H. M.; Adame, J. A. A.; Rojas-López, M. Morphological and Optical Characterization of Gold Nanoparticles Decorated Porous Silicon. *J. Nanosci. Nanotechnol.* **2019**, *19* (6), 3604−3609.
(11) Alwan, A. M.; Naseef, I. A. Optimization of Photoluminescence Properties of Porous Silicon by Adding Gold Nanoparticles. *Iraqi J. Sci.* **2017**, *58*, 53-62.
(12) Escobar, S.; Nava, R.; Reyes-Esqueda, J. A. Plasmonic-Enhanced Photoluminescence in Porous Silicon with Pore-Embedded Gold Nanoparticles Fabricated by Direct Reduction of Chloroauric Acid. Available at SSRN: https://ssrn.com/abstract=4648792, Accessed 3 June 2025.
(13) Jin, Y.; Yang, Y.; Duan, W.; Qu, X.; Wu, J. Synergistic and On-Demand Release of Ag-AMPs Loaded on Porous Please provide page number for Refs 9 and 11.Silicon Nanocarriers for Antibacteria and Wound Healing. *ACS Appl. Mater. Interfaces* **2021**, *13* (14), 16127−16141.
(14) Lee, E. M.; Lee, J.; Kim, Y.; Yi, K. S.; Cho, J.; Kim, J.; An, J. M.; Lee, D.; Kim, S. J.; An, E.; Hong, Y. J.; Jo, H.; Lee, S. H.; Jung, Y.; Choi, C.-H.; Kang, J. S.; Hur, J.; Kim, D. Hybrid Composite of Silver Nanoparticle−Porous Silicon Microparticles as an Image-Guided Localization Agent for Computed Tomography Scan of the Lungs. *ACS Biomater. Sci. Eng.* **2020**, *6* (8), 4390−4396.
(15) Jiao, Y.; Koktysh, D. S.; Phambu, N.; Weiss, S. M. Dual-Mode Sensing Platform Based on Colloidal Gold Functionalized Porous Silicon. *Appl. Phys. Lett.* **2010**, *97* (15), 153125.
(16) Bandarenka, H. V.; Girel, K. V.; Zavatski, S. A.; Panarin, A.; Terekhov, S. N. Progress in the Development of SERS-Active Substrates Based on Metal-Coated Porous Silicon. *Materials* **2018**, *11* (5), 852.
(17) Chan, S.; Berlin, A. A.; Yamakawa, M. Metal Coated Nanocrystalline Silicon as an Active Surface Enhanced Raman Spectroscopy (SERS) Substrate. US6970239 B2, November 29, 2005.
(18) Bu, Y.; Zhu, G.; Li, S.; Qi, R.; Bhave, G.; Zhang, D.; Han, R.; Sun, D.; Liu, X.; Hu, Z.; Liu, X. Silver-Nanoparticle-Embedded Porous Silicon Disks Enabled SERS Signal Amplification for Selective Glutathione Detection. *ACS Appl. Nano Mater.* **2018**, *1* (1), 410−417.
(19) Zeiri, L.; Rechav, K.; Porat, Z.; Zeiri, Y. Silver Nanoparticles Deposited on Porous Silicon as a Surface-Enhanced Raman Scattering (SERS) Active Substrate. *Appl. Spectrosc.* **2012**, *66* (3), 294−299.
(20) Ismail, N. F.; Lee, K. Y.; Mohd Hadis, N. S.; Ismail, L. N.; Abdul Rahim, A. F.; Abdullah, M. H.; Radzol, A. R. M. Nano Silver-Coated Porous Silicon-Based Surface-Enhanced Raman Spectroscopy Substrate for Low-Concentration Dengue NS1 Protein Detection. *J. Appl. Spectrosc.* **2024**, *91* (2), 480−488.
(21) Vendamani, V. S.; Beeram, R.; Nageswara Rao, S. V. S.; Pathak, A. P.; Soma, V. R. Trace Level Detection of Explosives and Pesticides Using Robust, Low-Cost, Free-Standing Silver Nanoparticles Decorated Porous Silicon. *Opt. Express* **2021**, *29* (19), 30045.
(22) Vo, V.-T.; Gwon, Y.; Phung, V.-D.; Son, Y.-D.; Kim, J.-H.; Lee, S.-W. Ag-Deposited Porous Silicon as a SERS-Active Substrate for the Sensitive Detection of Catecholamine Neurotransmitters. *Electron. Mater. Lett.* **2021**, *17* (3), 292−298.
(23) Ma, X.; Cheng, H.; Hou, J.; Jia, Z.; Wu, G.; Lü, X.; Li, H.; Zheng, X.; Chen, C. Detection of Breast Cancer Based on Novel Porous Silicon Bragg Reflector Surface-Enhanced Raman Spectroscopy-Active Structure. *Chin. Opt. Lett.* **2020**, *18* (5), 051701.
(24) Li, H.; Wang, Q.; Gao, N.; Fu, J.; Yue, X.; Lv, X.; Zhong, F.; Tang, J.; Wang, T. Facile Synthesis of Magnetic Ionic Liquids/Gold Nanoparticles/Porous Silicon Composite SERS Substrate for Ultra-Sensitive Detection of Arsenic. *Appl. Surf. Sci.* **2021**, *545*, 148992.
(25) Škrabić, M.; Krajačić, M.; Gotić, M.; Baran, N.; Mikac, L.; Jurkin, T.; Šegedin, N.; Ivanda, M.; Gamulin, O. Gold-Coated Porous Silicon as a SERS Substrate for near-Infrared Excitation: Off- and on-Resonant Conditions. *Appl. Surf. Sci.* **2024**, *644*, 158820.
(26) Mariani, S.; Paghi, A.; La Mattina, A. A.; Debrassi, A.; Dähne, L.; Barillaro, G. Decoration of Porous Silicon with Gold Nanoparticles via Layer-by-Layer Nanoassembly for Interferometric and Hybrid Photonic/Plasmonic (Bio)Sensing. *ACS Appl. Mater. Interfaces* **2019**, *11* (46), 43731−43740.
(27) Khinevich, N.; Bandarenka, H.; Zavatski, S.; Girel, K.; Tamulevičienė, A.; Tamulevičius, T.; Tamulevičius, S. Porous Silicon - A Versatile Platform for Mass-Production of Ultrasensitive SERS-Active Substrates. *Microporous Mesoporous Mater.* **2021**, *323*, 111204.
(28) Rashed, Md. A.; Harraz, F. A.; Faisal, M.; El-Toni, A. M.; Alsaiari, M.; Al-Assiri, M. S. Gold Nanoparticles Plated Porous Silicon Nanopowder for Nonenzymatic Voltammetric Detection of Hydrogen Peroxide. *Anal. Biochem.* **2021**, *615*, 114065.
(29) Jasim, M. H.; Nayef, U. M.; Hussien, H. T. Study of Spectral Responsivity of Au@In2O3 Nanoparticles via Laser Ablation Deposited on Porous Silicon. *Plasmonics* **2024**, *19* (2), 933−941.
(30) Bardet, B.; Desplobain, S.; Billoué, J.; Ventura, L.; Gautier, G. Integration of Low-Loss Inductors on Thin Porous Silicon Membranes. *Microelectron. Eng.* **2018**, *194*, 96−99.
(31) Sailor, M. J. *Porous Silicon in Practice: Preparation, Characterization and Applications*; Wiley VCH: Weinheim, Germany, 2011; ISBN 978−3-527−31378−5.
(32) Solanki, C. S.; Bilyalov, R. R.; Poortmans, J.; Celis, J.-P.; Nijs, J.; Mertens, R. Self-Standing Porous Silicon Films by One-Step Anodizing. *J. Electrochem. Soc.* **2004**, *151* (5), C307.
(33) Chen, I.-T.; Sessoms, D. A.; Sherman, Z.; Choi, E.; Vincent, O.; Stroock, A. D. Stability Limit of Water by Metastable Vapor−Liquid Equilibrium with Nanoporous Silicon Membranes. *J. Phys. Chem. B* **2016**, *120* (23), 5209−5222.
(34) Goryachev, D. N.; Belyakov, L. V.; Sreseli, O. M. Free-Standing Luminescent Layers of Porous Silicon. *Semiconductors* **2010**, *44* (12), 1588−1591.

(35) Thakur, M.; Pernites, R. B.; Nitta, N.; Isaacson, M.; Sinsabaugh, S. L.; Wong, M. S.; Biswal, S. L. Freestanding Macroporous Silicon and Pyrolyzed Polyacrylonitrile As a Composite Anode for Lithium Ion Batteries. *Chem. Mater.* **2012**, *24* (15), 2998−3003.
(36) Ning, H.; Krueger, N. A.; Sheng, X.; Keum, H.; Zhang, C.; Choquette, K. D.; Li, X.; Kim, S.; Rogers, J. A.; Braun, P. V. Transfer-Printing of Tunable Porous Silicon Microcavities with Embedded Emitters. *ACS Photon.* **2014**, *1* (11), 1144−1150.
(37) Chiadò, A.; Novara, C.; Lamberti, A.; Geobaldo, F.; Giorgis, F.; Rivolo, P. Immobilization of Oligonucleotides on Metal-Dielectric Nanostructures for miRNA Detection. *Anal. Chem.* **2016**, *88* (19), 9554−9563.
(38) Novara, C.; Lamberti, A.; Chiadò, A.; Virga, A.; Rivolo, P.; Geobaldo, F.; Giorgis, F. Surface-Enhanced Raman Spectroscopy on Porous Silicon Membranes Decorated with Ag Nanoparticles Integrated in Elastomeric Microfluidic Chips. *RSC Adv.* **2016**, *6* (26), 21865−21870.
(39) Novara, C.; Chiadò, A.; Paccotti, N.; Catuogno, S.; Esposito, C. L.; Condorelli, G.; De Franciscis, V.; Geobaldo, F.; Rivolo, P.; Giorgis, F. SERS-Active Metal-Dielectric Nanostructures Integrated in Microfluidic Devices for Label-Free Quantitative Detection of miRNA. *Faraday Discuss.* **2017**, *205*, 271−289.
(40) Martin-Sanchez, D.; Ponce-Alcantara, S.; Garcia-Ruperez, J. Sensitivity Comparison of a Self-Standing Porous Silicon Membrane Under Flow-Through and Flow-Over Conditions. *IEEE Sensors J.* **2019**, *19* (9), 3276−3281.
(41) Wan, Y.; Krueger, N. A.; Ocier, C. R.; Su, P.; Braun, P. V.; Cunningham, B. T. Resonant Mode Engineering of Photonic Crystal Sensors Clad with Ultralow Refractive Index Porous Silicon Dioxide. *Adv. Opt. Mater.* **2017**, *5* (21), 1700605.
(42) Corsi, M.; Paghi, A.; Mariani, S.; Golinelli, G.; Debrassi, A.; Egri, G.; Leo, G.; Vandini, E.; Vilella, A.; Dähne, L.; Giuliani, D.; Barillaro, G. Bioresorbable Nanostructured Chemical Sensor for Monitoring of pH Level In Vivo. *Adv. Sci.* **2022**, *9* (22), 2202062.
(43) Zhao, Y.; Gaur, G.; Retterer, S. T.; Laibinis, P. E.; Weiss, S. M. Flow-Through Porous Silicon Membranes for Real-Time Label-Free Biosensing. *Anal. Chem.* **2016**, *88* (22), 10940−10948.
(44) Meade, S. O.; Sailor, M. J. Microfabrication of Freestanding Porous Silicon Particles Containing Spectral Barcodes. *Phys. Status Solidi RRL* **2007**, *1* (2), R71.
(45) Ivanov, A. *Silicon Anodization as a Structuring Technique*; Springer Fachmedien Wiesbaden: Wiesbaden, 2018..
(46) Ivanov, A.; Mescheder, U.; Woias, P. Finite-Elements Simulation of Etch Front Propagation in Silicon Electropolishing Process. *ECS Trans.* **2014**, *58* (46), 15−24.
(47) Engel, A.; Drault, F.; Demoustier-Champagne, S. M.; Hermans, S. High Yield Au Nanorods Synthesis: Investigation of the Synthesis Parameters Tunability by Statistical Methods. *Langmuir* **2025**, *41* (25), 15805−15818.
(48) Jana, N. R.; Gearheart, L.; Murphy, C. J. Seed-Mediated Growth Approach for Shape-Controlled Synthesis of Spheroidal and Rod-like Gold Nanoparticles Using a Surfactant Template. *Adv. Mater.* **2001**, *13* (18), 1389−1393.
(49) Zheng, J.; Cheng, X.; Zhang, H.; Bai, X.; Ai, R.; Shao, L.; Wang, J. Gold Nanorods: The Most Versatile Plasmonic Nanoparticles. *Chem. Rev.* **2021**, *121* (21), 13342−13453.
(50) Li, G. V.; Astrova, E. V.; Preobrazhenskii, N. E.; Rumyantsev, A. M.; Pavlov, S. I.; Beregulin, E. V. Negative Electrodes for Lithium-Ion Batteries Obtained by Photoanodization of Solar-Grade Silicon. *Technol. Phys.* **2019**, *64* (5), 660−665.
(51) Lysenko, V.; Vitiello, J.; Remaki, B.; Barbier, D. Gas Permeability of Porous Silicon Nanostructures. *Phys. Rev. E* **2004**, *70* (1), 017301.
(52) Astrova, E. V.; Tolmachev, V. A. Effective Refractive Index and Composition of Oxidized Porous Silicon Films. *Mater. Sci. Eng.: B* **2000**, *69*−*70*, 142−148.
(53) Terheiden, B.; Hensen, J.; Wolf, A.; Horbelt, R.; Plagwitz, H.; Brendel, R. Layer Transfer from Chemically Etched 150 Mm Porous Si Substrates. *Materials* **2011**, *4* (5), 941−951.
(54) Jubgang Fandio, D. J.; Sauze, S.; Boucherif, A.; Arès, R.; Morris, D. Structural, Optical and Terahertz Properties of Graphene-Mesoporous Silicon Nanocomposites. *Nanoscale Adv.* **2020**, *2* (1), 340−346.
(55) Liu, R.; Schmedake, T. A.; Li, Y. Y.; Sailor, M. J.; Fainman, Y. Novel Porous Silicon Vapor Sensor Based on Polarization Interferometry. *Sens. Actuators, B* **2002**, *87* (1), 58−62.
(56) De La Luz-Merino, S.; Calixto, Ma. E.; Méndez-Blas, A. Nanostructured CuInSe2 by Electrodeposition with the Assistance of Porous Silicon Templates. *Mater. Chem. Phys.* **2015**, *163*, 362−368.
(57) Velleman, L.; Shearer, C. J.; Ellis, A. V.; Losic, D.; Voelcker, N. H.; Shapter, J. G. Fabrication of Self-Supporting Porous Silicon Membranes and Tuning Transport Properties by Surface Functionalization. *Nanoscale* **2010**, *2* (9), 1756.
(58) Cencha, L. G.; Antonio Hernández, C.; Forzani, L.; Urteaga, R.; Koropecki, R. R. Optical Performance of Hybrid Porous Silicon−Porous Alumina Multilayers. *J. Appl. Phys.* **2018**, *123* (18), 183101.
(59) Pei, Y.; Shahoei, S. H.; Li, Y.; Reece, P. J.; Nelson, E. R.; Gooding, J. J.; Kilian, K. A. Vertical Integration of Cell-Laden Hydrogels with Bioinspired Photonic Crystal Membranes. *Adv. Mater. Interfaces* **2018**, *5* (23), 1801233.

https://doi.org/10.1021/acsanm.5c03632
ACS Appl. Nano Mater. 2025, 8, 21285−21293